Appl. Chem. Eng., Vol. 29, No. 5, October 2018, 626-629
https://doi.org/10.14478/ace.2018.1088

Article

외부 유입 가스 조절을 통한 연료전지 구동 성능 안정화

장한샘 · 박영은 · 이재영†

광주과학기술원 지구·환경공학부, Ertl 탄소비움연구센터
(2018년 8월 22일 접수, 2018년 9월 5일 심사, 2018년 9월 6일 채택)

An Experimental Guide to Predictable Fuel Cell Operations by Controlling External Gas Supply

Hansaem Jang, Youngeun Park, and Jaeyoung Lee†

School of Earth Sciences and Environmental Engineering, Ertl Center for Electrochemistry and Catalysis, Gwangju Institute of Science and Technology (GIST), 123 Cheomdan-gwagiro, Buk-gu, Gwangju 61005, Korea
(Received August 22, 2018; Revised September 5, 2018; Accepted September 6, 2018)

초 록

연료전지는 높은 연료유연성을 갖고 있어, 탄소 및 탄화수소 등을 통해서도 전기를 생산할 수 있다. 하지만 이러한 연료원을 사용한 경우, 불안정한 장기 구동성능이 종종 관측된다. 본 연구에서는 반응기 내부에 존재하는 탄화수소가 장기 구동성능을 불안정하게 함을 밝힌다. 본 연구진은 비활성기체인 아르곤을 이용하여 산화극 반응기 내부의 가스화 경로를 예측하고, 이를 통해 탄화수소의 영향을 억제하여 불안정한 장기 구동성능을 극복한다. 더 나아가, 산화극 반응기 내부에 이산화탄소를 공급하여 역부드아반응을 유도한다. 역부드아반응을 통해 탄소연료전지에서 연료로 사용될 수 있는 일산화탄소를 만들어낸다. 과도한 이산화탄소의 주입은 오히려 연료손실 등의 문제를 야기함을 확인한다. 따라서, 본 연구에서는 이산화탄소 공급량의 최적화가 중요함을 밝히고, 이를 통해 연료전지 구동 성능을 안정화한다.

Abstract

Fuel cell is one of the promising electrochemical technologies enabling power production with various fuel sources such as hydrogen, hydrocarbon and even solid carbon. However, its long-term performance is often unstable and unpredictable. In this work, we observed that gasification-driven hydrocarbons were the culprit of unpredictability. Therefore, we controlled the presence of hydrocarbons with the help of external gas supply, *i.e.* argon and carbon dioxide, and suggested the optimal amount of carbon dioxide required for predictable fuel cell operations. Our optimization strategy was based upon the following observations; carbon dioxide can work as both an inert gas and a fuel precursor, depending on its amount present in the reactor. When deficient, the carbon dioxide cannot fully promote the reverse Boudouard reaction that produces carbon monoxide fuel. When overly present, the carbon dioxide works as an inert gas that causes fuel loss. In addition, the excessive carbon monoxide may result in coking on the catalyst surface, leading to the decrease in the power performance.

Keywords*: solid electrolyte, fuel cell, external gas, Boudouard reaction, carbon*

1. Introduction

Solid oxide carbon fuel cells (SO-CFCs) have been traditionally thought as the system that generates electricity based on the equations below (Eqs. 1-5). This system involves a direct conversion of solid-state carbon into either carbon dioxide with a 4 electron transfer reaction or carbon monoxide with a 2 electron reaction. The system also includes the electrochemical oxidation of carbon monoxide that produces 2 electrons, since carbon monoxide is further oxidizable with oxygen as hydrogen or hydrocarbons are in solid oxide fuel cells. In SO-CFCs, carbon monoxide is generally believed to originate from either a partial electrochemical oxidation of solid carbon (Eq. 3) or the reverse Boudouard reaction (Eq. 6).

$$\text{Overall: } C + O_2 \rightarrow CO_2 \quad (1)$$

$$\text{Anode: } C + 2O^{2-} \rightarrow CO_2 + 4e^- \quad (2)$$

$$\text{Anode: } C + O^{2-} \rightarrow CO + 2e^- \quad (3)$$

† Corresponding Author: School of Earth Sciences and Environmental Engineering, Ertl Center for Electrochemistry and Catalysis, Gwangju Institute of Science and Technology (GIST), 123 Cheomdan-gwagiro, Buk-gu, Gwangju 61005, Korea
Tel: +82-62-715-2440 e-mail: jaeyoung@gist.ac.kr

pISSN: 1225-0112 eISSN: 2288-4505

Table 1. Description on Experimental Conditions of Gas Supply to the Anode Chamber

Flow Gas	Flow Rate (sccm)	Abbreviation	Expected Outcome		
			IG_{EF}	IG_{CS}	IG_{TPB}
–	0	*0flow*	–	Unaffected	Unaffected
Ar	50	*50Ar*	–	Affected	Affected
CO_2	25	*25CO₂*	Affected	Affected	Unaffected
CO_2	50	*50CO₂*	Affected	Affected	Unaffected
CO_2	100	*100CO₂*	Affected	Affected	Unaffected

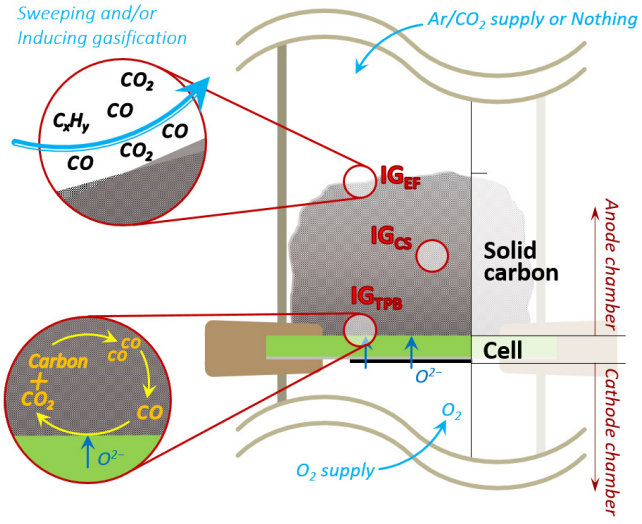

Figure 1. Schematic illustration of the three gasification pathways possibly occurring within an anode chamber in solid oxide carbon fuel cells.

$$\text{Anode: } CO + O^{2-} \rightarrow CO_2 + 2e^- \quad (4)$$

$$\text{Cathode: } O_2 + 4e^- \rightarrow 2O^{2-} \quad (5)$$

$$\text{Anode: } C + CO_2 \leftrightarrow 2CO \quad (6)$$

Recent studies show that it is not solid state carbon that actually serves as fuel in SO-CFCs, but further oxidizable gaseous molecules (or actual fuel hereinafter) which are produced via gasification reactions with solid carbon[1-5], including the reverse Boudouard reaction (Eq. 6). However a reaction mechanism of SO-CFCs is not exactly identical to the other gas-powered solid oxide based fuel cells. First the number of actual fuel reaching triple phase boundaries (TPBs) in SO-CFCs is finite unless otherwise specially treated for further gasification; the lack of fuel causes oxidation of Ni electrocatalyst and eventually cracks the cell. Second the major contribution of fuel in SO-CFCs is not H_2 or hydrocarbons but CO, which can poison electrocatalyst surfaces by coking. Thus it is imperative to keep the balance of the amount of actual fuel in SO-CFCs, thereby securing catalytic activity.

2. Experimental

Our goal is to make fuel cell operations more predictable based on knowledge on gasification. As described in the Introduction section, there are three major gasification pathways available in SO-CFCs: IG_{EF} (internal gasification near triple phase boundaries; most likely CO shuttle mechanism), IG_{CS} (internal gasification by carbon source itself) and IG_{TPB} (internal gasification with external flow). Schematic illustration of gasification pathways is represented in Figure 1. Generally IGCS accompanies substantial formation of hydrocarbons and therefore is considered the culprit of unexpected power performances, behind which there are two reasons. First hydrocarbons cannot be formed once intrinsic impurities or moisture within carbon is consumed, and thus is regarded as a finite source of fuel. Second, because all chemicals have their own open circuit voltages (OCVs) when oxidized, the state of mixture complicates the voltage prediction. Thus our goal now is to suppress IGCS while promoting the other pathways to produce CO by providing CO_2 which acts as a precursor to CO during the reverse Boudouard reaction at the temperatures beyond *ca.* 700 ℃[6].

In order to deal solely with IG_{EF}, we selected Ensaco 350G (Timcal) as a carbon source which is reported to show a balanced IG_{CS} rate, and set the oxygen flow rate to 50 sccm (standard cm^3/min) which is known to have an optimal IG_{TPB} rate when running with Ensaco 350G [7]. The materials preparation procedure for this work is the same as our previous work[7], except the fact that we used 900 mg of a carbon source in this experiments. It should be noted that the volume of our anode chamber is 195 cm^3 with a cylindrical shape. We chose Ar and CO_2 as an external flow gas because they have absolutely different features each other, and we conducted our experiments as described in Table 1. During each experiment, we sampled the gas production from the anode chamber exhaust stream with a syringe and then analyzed the contents by mass spectrometry (5975C, Agilent Technoloies). Also, we measured the high frequency resistance of an operating cell by AC-impedance meter (1 kHz, 2,560 AC mΩ HiTester, Hioki).

3. Results and Discussion

Three different strategies can be taken for balancing the amount of actual fuel. The first strategy is to manipulate the amount of oxide ions reaching the anode. The second is to select a proper carbon source that is not too reactive or too sluggish for gasification. The last is to take advantage of an external gas inflow toward the carbon source in order

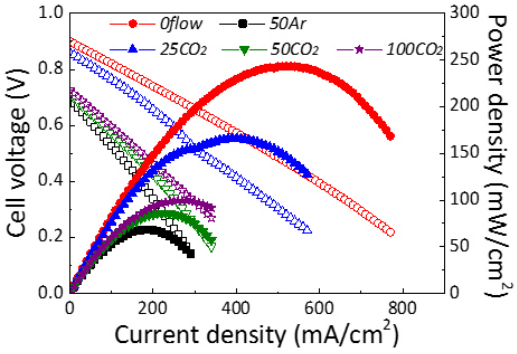

Figure 2. Short-term power performance result represented by polarization curves.

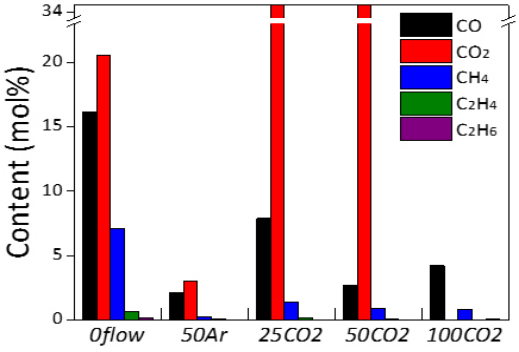

Figure 3. Gas chromatograms of all the experimental sets taken before a short-term power performance test. Please note the CO_2 value of *100CO₂* is thought to exceed the detection limit.

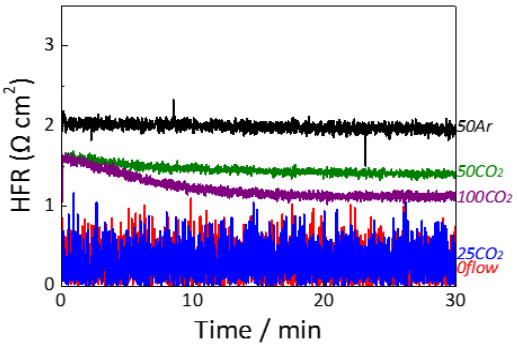

Figure 4. High frequency resistance result during a long-term power performance test. Please note that all experiments were carried out at a mid-range setting.

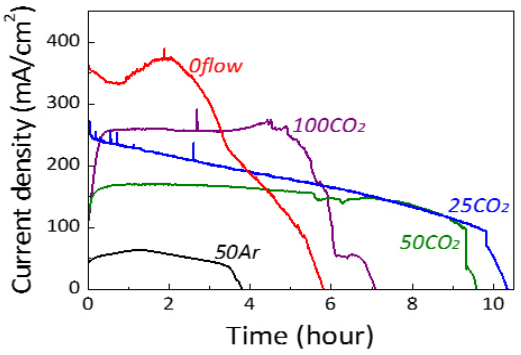

Figure 5. Long-term power performance by discharge test under a constant voltage of 0.6 V. Note: the total charge of each test is 1489.4 mAh (*0flow*), 194.3 mAh (*50Ar*), 1756.1 mAh (*25CO₂*), 1435.3 mAh (*50CO₂*) and 913.3 mAh (*100CO₂*).

to control gasification. These three strategies are respectively related to three different gasification pathways that can occur during fuel cell operations (Figure 1): internal gasification near triple phase boundaries (IG_{TPB}; most likely CO shuttle mechanism[8]); internal gasification by carbon source itself (IG_{CS}; [7]); internal gasification with external flow (IG_{EF}; reverse Boudouard reaction, steam gasification[9-15]). In a previous publication[7], we successfully optimized fuel cell operations by controlling IG_{TPB} and IG_{CS}. Here we deal with IG_{EF} and propose an experimental guide to predictable fuel cell operations.

Polarization curves in Figure 2 show that *0flow* exhibits the highest maximum power density (MPD) as well as the shallowest slope in a mass transport losses curve, followed by *25CO₂*, *100CO₂*, *50CO₂* and *50Ar*. An MPD, or a peak power density, is a power density value at the point of inflection of a curve. Under the same cell materials and the same program settings being employed, it is mass transport losses that govern steepness of a slope. Taken together, we can predict that the amount of actual fuel would be like *0flow* > *25CO₂* > *100CO₂* > *50CO₂* > *50Ar*. Interestingly, this order holds also for OCVs. Theoretical OCVs for hydrocarbon oxidations are generally higher than CO oxidation, which suggests that the higher OCV, the higher proportion of hydrocarbons within an anode chamber. Thus we can predict the content of hydrocarbon would be like *0flow* > *25CO₂* >> *100CO₂* ≥ *50CO₂* > *50Ar*.

Gas chromatography can validate the aforementioned predictions. According to gas chromatograms in Figure 3, actual fuel is formed most abundantly in *0flow*, followed by *25CO₂*, *100CO₂*, *50CO₂* and *50Ar*. Also, as expected, hydrocarbons are formed most abundantly in *0flow*, followed by *25CO₂*, *100CO₂*, *50CO₂* and *50Ar*.

Considering the hydrocarbons content of *50Ar* (Figure 3), 50 sccm is a sufficient flow rate to purge the chamber. However hydrocarbons are still detectable in case of *50CO₂* and *100CO₂*. It implies that the provided CO_2 is involved with hydrocarbon formation gasification reactions. It is also interesting to note that although Ar is supplied, CO can be formed (Figure 3, *50Ar*). It suggests that regardless of an external gas inflow, IG_{TPB} occurs to a certain extent. Unlike Ar inflow, CO_2 inflow allows hydrocarbon to be formed. In Figure 3, *0flow* shows the highest amount of hydrogen source (hydrocarbons), followed by *25CO₂*, *100CO₂*, *50CO₂* and *50Ar*. When running with higher hydrogen ratio, Ni electrocatalyst is less prone to coking[16] and CO is the major contribution to coking[10]. It is also reported that once electric load is added, coking can be removed[7]. These reports are in excellent agreement with Figure 4. In Figure 4, *0flow* and *25CO₂* show unmeasurably lower high frequency resistances (HFRs) than the others. It should be noted that HFR was measured at a mid-range (ohm scale) setting where it is inaccurate to measure a milliohm (or lower) scale HFR, and it is the reason *25CO₂* and *0flow* come with strong noises

in Figure 4. When it comes to the other three sets, the HFR curves show a decreasing trend after electric load is applied. It is because the applied load eventually leads to the removal of coking on the electrocatalyst surfaces. In line with the decreasing trend of the HFR curves, the other three's current density values start to increase after applying electric load as shown in Figure 5.

The key for predictable fuel cell operations is whether or not it has consistent power performance with respect to time. That is, desirable is a curve that has the most shallowest slope at plateau in Figure 5. In this regard, *100CO₂* and *50CO₂* can be declared as predictable operation conditions (Figure 5). Considering the total charge of each test which is specified in the Figure 5 caption, however, *100CO₂* has significant actual fuel losses. Thus, it is recommended not to choose conditions like *100CO₂* unless higher current density is strongly required at a fixed voltage applied.

4. Conclusions

There are two elements to consider when aiming at predictable SO-CFC operations. One is how to suppress the hydrocarbons present inside the reactor; hydrocarbon is a finite source of fuel and complexes theoretical voltage calculations. The other is how to promote CO formation in a balanced manner; poisoning on electrocatalyst can occur not only when CO production is excessive, but also when it is deficient. Leveraging the knowledge on gasification pathways, we have successfully figured out that both inert and reactive external gas supply can control the hydrocarbons inside the reactor, thereby resulting in consistent power performance with respect to time. Although an overdose of CO_2 produces an excess of CO and then causes coking on electrocatalyst surfaces, coking can be easily removed during fuel cell operations by adding electric load on the cell. Eventually, a CO_2 overdose could enhance power performances - this prediction is considered valid until the number of CO produced is less than the number of oxide ions reaching TPBs. Nevertheless the overdose must be considered with extreme caution, since it leads to significant fuel losses.

Acknowledgement

This work was supported by the project R16EA01 of Korea Electric Power Corporation (KEPCO).

References

1. H. Jang, Y. Park, and J. Lee, Meticulous insight on the state of fuel in a solid oxide carbon fuel cell, *Chem. Eng. J.*, **308**, 974-979 (2017).
2. A. C. Chien, M. I. Petra, and C. M. Lim, Effect of contact mode and flow rate on direct carbon solid oxide fuel cell, *J. Chem. Eng. Jpn.*, **49**, 362-365 (2016).
3. K. M. Ong and A. F. Ghoniem, Modeling of indirect carbon fuel cell systems with steam and dry gasification, *J. Power Sources*, **313**, 51-64 (2016).
4. S. Eom, S. Ahn, Y. Rhie, K. Kang, Y. Sung, C. Moon, G. Ghoi, and D. Kim, Influence of devolatilized gases composition from raw coal fuel in the lab scale DCFC (direct carbon fuel cell) system, *Energy*, **74**, 734-740 (2014).
5. Y. Tang and J. Liu, Effect of anode and Boudouard reaction catalysts on the performance of direct carbon solid oxide fuel cells, *Int. J. Hydrogen Energy*, **35**, 11188-11193 (2010).
6. H. Jang, J. D. Ocon, S. Lee, J. K. Lee, and J. Lee, Direct power generation from waste coffee grounds in a biomass fuel cell, *J. Power Sources*, **296**, 433-439 (2015).
7. H. Jang, Y. Park, and J. Lee, Origin of peculiar electrochemical phenomena in direct carbon fuel cells, *Chem. Eng. J.*, **327**, 1163-1175 (2017).
8. T. M. Gur, Mechanistic modes for solid carbon conversion in high temperature fuel cells, *J. Electrochem. Soc.*, **157**, B751-B759 (2010).
9. W. H. A. Peelen, M. Olivry, S. F. Au, J. D. Fehribach, and K. Hemmes, Electrochemical oxidation of carbon in a 62/38 mol% Li/K carbonate melt, *J. Appl. Electrochem.*, **30**, 1389-1395 (2000).
10. T. M. Gur, Critical review of carbon conversion in "carbon fuel cells", *Chem. Rev.*, **113**, 6179-6206 (2013).
11. T. Wall, Y. Liu, C. Spero, L. Elliott, S. Khare, R. Rathnam, F. Zeenathal, B. Moghtaderi, B. Buhre, C. Sheng, R. Gupta, T. Yamada, K. Makino, and J. Yu, An overview on oxyfuel coal combustion-State of the art research and technology development, *Chem. Eng. Res. Des.*, **87**, 1003-1016 (2009).
12. R. E. Mitchell, L. Ma, and B. Kim, On the burning behavior of pulverized coal chars, *Combust. Flame*, **151**, 426-436 (2007).
13. P. A. Campbell, R. E. Mitchell, and L. Ma, Characterization of coal char and biomass char reactivities to oxygen, *Proc. Combust. Inst.*, **29**, 519-526 (2002).
14. W. A. Kneller, Physicochemical characterization of coal and coal reactivity: A review, *Thermochim. Acta*, **108**, 357-388 (1986).
15. N. M. Laurendeau, Heterogeneous kinetics of coal char gasification and combustion, *Prog. Energy Combust. Sci.*, **4**, 221-270 (1978).
16. J.-H. Koh, Y.-S. Yoo, J.-W. Park, and H. C. Lim, Carbon deposition and cell performance of Ni-YSZ anode support SOFC with methane fuel, *Solid State Ion.*, **149**, 157-166 (2002).